This document is the accepted manuscript version of the following article:
Prendin, A. L., Petit, G., Fonti, P., Rixen, C., Dawes, M. A., & von Arx, G. (2018). Axial xylem architecture of Larix decidua exposed to CO2 enrichment and soil warming at the tree line. Functional Ecology, 32(2), 273-287. https://doi.org/10.1111/1365-2435.12986

Axial xylem architecture of *Larix decidua* exposed to CO_2 enrichment and soil warming at the treeline

Angela Luisa Prendin[a*], Giai Petit[a], Patrick Fonti[b], Christian Rixen[c], Melissa Autumn Dawes[b,c], Georg von Arx[b,d]

[a] Dept. Territorio e Sistemi Agro-Forestali, Università degli Studi di Padova, Legnaro (PD), Italy

[b] Swiss Federal Institute for Forest, Snow and Landscape Research WSL, Birmensdorf, Switzerland

[c] WSL Institute for Snow and Avalanche Research SLF, Davos, Switzerland

[d] Climatic Change and Climate Impacts, Institute for Environmental Sciences, Geneva, Switzerland

[*] Corresponding author: angelaluisa.prendin@studenti.unipd.it

Running headline: Axial xylem architecture at increased [CO_2] and soil temperature

Summary

1. Trees continuously adjust their axial xylem structure to meet changing needs imposed by ontogenetic and environmental changes. These axial structure-function responses need to be coordinated among competing biophysical constraints to avoid failure of the xylem system. Here, we investigated if ontogeny or experimental manipulation of CO_2 and soil temperature influence these structure-function responses.
2. We performed detailed xylem cell anatomical quantification along the axis of 40-year-old *Larix decidua* trees planted at the Swiss treeline and exposed to a combination of elevated CO_2 (+200 ppm) and soil warming (+4 °C) between 2001 and 2012. We assessed how mean hydraulic tracheid diameter (*Dh*), the cell wall reinforcement ($(t/b)^2$), tracheid wall thickness (*CWT*) and the percent area of ray parenchyma (*PERPAR*) – proxies for hydraulic efficiency, hydraulic safety, biomechanical support and metabolic xylem functions, respectively – co-vary along the tree axis.
3. *Dh* increased from the stem apex to base, strictly following a power function (R^2=0.81), independent from ontogeny and experimental treatments. In contrast, axial trends of $(t/b)^2$ and *CWT* were either influenced by treatment and/or ontogeny, or showed no axial trend (*PERPAR*). Additionally, we found that a larger *Dh* only at the stem apex promoted primary and secondary growth.
4. Our approach of analyzing xylem anatomical traits along the tree axis and across tree-rings provides novel insights into xylem functional architecture and allows reconstructing xylem function over time. We conclude that the maintenance of hydraulic efficiency during ontogeny is very robust, that the conduit diameter undergoes a strong apical control, and plays a fundamental role for assimilation and tree growth. Instead, the other functional traits more plastically vary with ontogeny and environmental changes.

Key-words: axial scaling, cell wall thickness, elevated CO_2, ray parenchyma, soil warming, structure-function relationships, tracheid lumen size, tree-ring anatomy

INTRODUCTION

Plants have developed different mechanisms to continuously adjust to environmental variability and changing needs and priorities. Short-term responses of physiological processes at different organizational levels are common to all plant types. However, especially for long-living trees that continuously increase in size and biomass, profound structural adjustments are necessary to meet changing requirements for transport, support and storage. In addition, many of these structural adjustments allow trees to acclimate to environmental variability and therefore to live for centuries or even millennia. Conversely, the legacy of past structural adjustments can constrain future responses of physiological processes (Meinzer, Lachenbruch & Dawson 2011; Anderegg *et al.* 2013). Thus, investigating how tree structures and their associated functions change over time and in relation to environmental variability provides a deeper understanding of tree growth and its determinants, which will ultimately help improve predictions of how forest ecosystems might be affected under different scenarios of climate change.

One emerging approach to gain such detailed structure-function insights is dendro-anatomy. Dendro-anatomy focuses on the quantitative assessment of the xylem tissues and cells, and the metrics or traits that can be derived and linked to specific xylem functions. The approach is based on the fact that xylem structural adjustments are permanently recorded and chronologically archived in the tree rings (Fonti *et al.* 2010), thus providing an explicit time frame in the retrospective analysis of the structure-function responses of trees to climate variability (Fonti & Jansen 2012). In conifers, the xylem is mainly composed of tracheids and parenchyma cells, both of which have multiple functional roles. Tracheids are axially-elongated cells that transport water from the roots to the canopy, provide mechanical support (Choat 2013; Bouche *et al.* 2014; Hacke 2015) and facilitate bending stiffness in the tree stem (Rosner & Karlsson 2011). In contrast, parenchyma cells are living cells that are predominantly organized as rays in conifers, running radially from the bark towards the pith, thus

physiologically integrating the xylem internally (Fonti *et al.* 2015) and with the phloem (Spicer 2014; Pfautsch, Hölttä & Mencuccini 2015). Collectively, parenchyma cells play a major role for storage and transport of water, nutrients (Beeckman 2016), and non-structural carbohydrates (NSC) (von Arx *et al.* 2017). In addition, parenchyma cells contribute in regulating the xylem hydraulics, e.g. through the osmo-regulation of axial and radial gradients of water potential (Brodersen & McElrone 2013; Lintunen *et al.* 2016) or by refilling embolized conductive elements (Salleo *et al.* 2009; Nardini, Lo Gullo & Salleo 2011; Ziemińska, Westoby & Wright 2015).

Quantifying how the dimensions and abundance of tracheids and parenchyma cells change within trees and in response to both increasing tree size and environmental variability might provide important insights into the plasticity of xylem functioning. Earlywood tracheids are thin-walled and characterized by wide lumina that contribute most to the efficiency of water transport (Domec & Gartner 2002). Hydraulic efficiency is commonly estimated by the xylem specific conductivity (Mencuccini, Grace & Fioravanti 1997) or by the hydraulic lumen diameter (Rosner & Karlsson 2011). While both of these metrics can be estimated from tracheid lumen properties, this approach ignores the fact that more than 60% of flow resistance resides in the tracheid walls as the water moves from one tracheid to the next through the bordered pit pores (Hacke 2015). However, the proportion of lumen vs. pit resistance seems to be more or less constant and independent from tracheid size (Pittermann *et al.* 2006). In contrast, the latewood tracheids with narrow lumina and thicker cell walls rather store water (Domec & Gartner 2002; Mcculloh *et al.* 2014) and, most importantly, provide biomechanical support (Koubaa, Zhang & Makni 2002; Finto, Schimleck & Daniels 2012). Indeed, the latewood cell wall thickness (*CWT*) is a key determinant for latewood density in conifers (Björklund *et al.* 2017). The latewood density strongly contributes to the overall wood density (Jyske, Mäkinen & Saranpää 2008), which is considered a good proxy for mechanical support and stiffness (Domec *et al.* 2009; Rosner & Karlsson 2011). Moreover the tracheid's thickness-to-span ratio, also referred to as cell wall reinforcement ($(t/b)^2$), is considered a primary determinant of the resistance to

hydraulic failure by implosion (Hacke *et al.* 2001; Pitterman et al. 2006). Hydraulic failure by implosion can occur when a water-filled conduit physically collapses owing to the pressure differences between its lumen and an adjacent air-filled conduit (Hacke *et al.* 2001). Both $(t/b)^2$ and percentage of latewood were shown to well correlate with embolism resistance in different organs (Domec *et al.* 2009) and across species (Bouche *et al.* 2014). The percentage of ray parenchyma can be used as a proxy for the amount of metabolically active tissue, with more parenchyma indicating greater vigour within a species (von Arx *et al.* 2015). Studying how characteristics of tracheids and abundance of parenchyma cells change within trees and in response to both increasing tree size and environmental variability might thus provide important insights into the plasticity of xylem functioning.

Our understanding of the variability of functionally relevant cell anatomical traits along the tree stem and root during ontogeny is still fragmentary. Theoretical models predict that different anatomical traits should vary according to strict allometric axial scaling defined by biophysical constraints that are related to tree size (West, Brown & Enquist 1999; Savage *et al.* 2010). Besides biophysical constraints, such as limiting the risk of hydraulic failure while maintaining an adequate capacity for water transport despite the increasing xylem tension with greater tree height (Domec *et al.* 2008), minimizing the carbon cost per unit leaf area may also be important (Olson *et al.* 2014). However, detailed empirical studies of within-plant patterns have mostly been limited to the axial variability of tracheid lumen diameter (but see Lazzarin *et al.* 2016). Both models and observations show that tracheid lumen diameter increases from the stem apex to the base following a power-like trajectory ($y=a \cdot x^b$), with a scaling exponent generally converging towards a value of ~0.2 irrespective of species, environment or ontogenetic stage (Anfodillo, Petit & Crivellaro 2013; Olson *et al.* 2014). This pattern is linked to the physical law of Hagen and Poiseuille, according to which hydraulic conductance increases with conduit lumen diameter to the fourth power (Tyree & Zimmermann 2002). Relatively small changes in tracheid lumen diameter therefore scale up to a large difference in xylem specific

127 conductivity. Consequently, the progressively wider conduits towards the base confine most of the
128 resistance and thus most of the tension within short distance from the apex (Petit & Anfodillo 2009).
129 This hydraulic architecture makes the pathway-length hydraulic resistance mostly independent from
130 tree height (West *et al.* 1999; Petit & Anfodillo 2009). In contrast, there is still little knowledge about
131 the axial variability of other important xylem structure-function relationships. A few empirical studies
132 have reported an increase in cell wall thickness (e.g., Myburg, Lev-Yadun & Sederoff 2013) with
133 increasing cambial age (Larson 1963; Mitchell & Denne 1997; Wimmer 2002, Lundgren, 2004),
134 likely following the pattern of *Dh*. While the cell wall reinforcement ($(t/b)^2$) decreased with tree age
135 but increased with height (Domec et al., 2009). A constant ray area and a decline of ray volume with
136 cambial age was found in previous studies (Bannan 1937; Gartner, Baker & Spicer 2000) but only
137 little information is available on the sensitivity of ray parenchyma tissue to environmental conditions
138 (Olano *et al.* 2013; Arx *et al.* 2017). Further, there is still a lack of knowledge about how these and
139 other functional traits co-vary both within the tree (e.g., Pittermann *et al.* 2006; Bouche *et al.* 2014;
140 Lachenbruch & McCulloh 2014) and over time, and thus we have only a limited understanding of
141 how competing biophysical constraints, functional priorities, and trade-offs are modulated by
142 ontogenetic development and environmental conditions (Gleason *et al.* 2016; Bittencourt, Pereira &
143 Oliveira 2016).
144
145 In this study, we retrospectively analysed the plasticity of functionally relevant xylem anatomical
146 traits along the tree axis. As a study framework, we selected an experimental site at an upper alpine
147 treeline. This temperature-limited ecotone is expected to be one of the terrestrial areas that is most
148 sensitive to climate change, and it has therefore become a focus of recent research (Harsch *et al.* 2009;
149 Körner 2012; Dawes *et al.* 2015). This is the reason why treelines are particularly suitable for
150 investigating the mechanisms of xylem growth responses to environmental changes (e.g., Petit *et al.*
151 2011; Fatichi *et al.* 2013; Fatichi, Leuzinger & Körner 2014). The treeline trees selected for this study
152 represent a subset of the 20 *L. decidua* exposed to a long-term experimental manipulation combining

153 free air CO_2 enrichment (FACE) and soil warming (Hättenschwiler *et al.* 2002; Dawes *et al.* 2015).
154 Previous analyses of *L. decidua* responses showed a stimulation of primary and secondary growth in
155 stems and roots by the CO_2 enrichment (Handa, Körner & Hättenschwiler 2006; Dawes *et al.* 2011,
156 2015), which was partially explained by a larger leaf canopy resulting in increased photosynthetic
157 carbon assimilation (Streit *et al.* 2014), while the experimental soil warming did not stimulate above-
158 or below-ground growth of *L. decidua* (Dawes *et al.* 2015). Building upon this knowledge from
159 previous studies at this site, we used a representative subset of the experimental *L. decidua* trees to
160 compare how the axial trends of four xylem functional traits related to hydraulic efficiency and safety,
161 biomechanical support, and metabolic requirements vary within annual rings from the stem apex to
162 the roots. In doing so, we specifically aimed to identify priorities and trade-offs among different
163 xylem functions and to determine if ontogeny or treatments influence these relationships. We
164 hypothesized that i) hydraulic traits are prioritized over mechanical traits, as the former seem to limit
165 tree height (Koch *et al.* 2004; Niklas & Spatz 2004; Niklas 2007); ii) there are trade-offs between
166 hydraulic efficiency and safety as approximated by cell wall reinforcement ($(t/b)^2$) at the within-ring
167 level because wide and thick-walled earlywood tracheids would require high carbon costs; and iii)
168 there are differences in trend plasticity, with the prioritized traits showing less plasticity during
169 ontogeny and in response to treatments.
170

171 ## MATERIALS AND METHODS

172

173 ### Study site, experimental setup and tree selection

174

175 The study included *Larix decidua* Miller trees from a long-term manipulation experiment located at
176 2180 m a.s.l., just above the current treeline (Barbeito *et al.* 2012), within the 40-year-old Stillberg
177 afforestation site near Davos, Switzerland (9°52'E, 46°46'N). The trees were on average 1.5 m tall in

178 2001 and 2.6 m in 2012 (Dawes *et al.* 2011) and spaced by >80 cm between stems of neighbouring
179 trees, surrounded by dense understory vegetation dominated by ericaceous dwarf shrubs
180 (Hättenschwiler *et al.* 2002; Dawes *et al.* 2015). The soil is classified as a Ranker (U.S. system: Lithic
181 Haplumbrept) with a 10-cm-deep organic top soil over siliceous bedrock (Paragneis, Schonenberger
182 & Frey 1988. Long-term average annual precipitation is 1,050 mm, mean maximum snow depth is
183 1.50 m, mean annual temperature is 1.4 °C, and average January and July temperatures are -5.8 °C
184 and 9.4 °C, respectively (Dawes *et al.* 2015). Climate conditions varied during the 4-year pre-
185 treatment period and the 9 years of experimental CO_2 enrichment (Dawes *et al.* 2011), but no
186 correlation was found between ring growth and the measured climate variables (Handa *et al.* 2006;
187 Dawes *et al.* 2011). The growing season starts approximately on 15 June with bud break of *L. decidua*
188 and ends on 25 September with needle senescence of *L. decidua*, thus lasting for c. 110 days
189 (Hättenschwiler *et al.* 2002). The manipulation experiment was performed between 2001 and 2012
190 and included different combinations of free air CO_2 enrichment (FACE) and soil warming (Table 1).
191 CO_2 enrichment (+200 ppm higher than ambient CO_2 concentration) was performed from 2001 to
192 2009 and soil warming (+4 °C at 5 cm depth) was applied using heating cables on the soil surface
193 (see Hättenschwiler *et al.* 2002; Hagedorn *et al.* 2010; Dawes *et al.* 2015 for details about the
194 experimental setup).
195
196 For this study, we used eight *L. decidua* trees, with two individuals per treatment combination: A_{2001},
197 A, EC, SW, ECSW, PECSW and PEC (Table 1). The study trees were selected to be representative
198 for the tree responses to each treatment based on previous results (see above), while considering the
199 presence of a leader shoot, lack of mechanical and/or herbivore damage, lack of snow mould, and
200 similar tree height at the beginning of the experiment.
201
202 **Reconstruction of axial and radial growth**
203

To capture the temporal variability of xylem anatomical traits along the stem axis, we reconstructed the apex-to-root axial trend within each tree ring to provide an annual resolution (Fig. S1). Thus, for each selected tree, we extracted a total of 20 discs along the stem (14) and the main root (6) (at 0-20 cm soil depth) for the reconstruction of both the axial and radial growth (Fig. S1). The average distance between neighbouring discs was 11 cm. Tree-ring widths were measured along eight equally spaced radii per disc and cross-dated to assign each ring to its year of formation. Annual stem and root elongation (ΔH) was obtained by linearly interpolating the inter-disc distance divided by the age difference between neighbouring discs:

$$\Delta H = \frac{H_i - H_{i-1}}{RN_{i-1} - RN_i} \qquad \text{eq. 1}$$

where H_i and RN_i are the height from the ground and the ring number of the i^{th} disc, respectively (Fig. S1). The average age difference between neighbouring discs varied from 1 to 14 years (with a median of 3 years) depending on the sample, thus giving reasonable confidence in the estimated annual stem elongation data (Fig. S1). Finally, to reconstruct the axial position at the time of ring formation, for each annual ring within a given disc we calculated the distance from the stem apex (L) as the difference between the reconstructed tree height and the distance from the ground (for root discs L was calculated as the sum of tree height and axial distance from the ground).

Anatomical measurements

Xylem cell anatomical measurements were performed using image analysis for a subset of the stem discs. In total we selected ten axially well-distributed discs per tree, six from the stem and four from the roots (Fig. S2). We followed the standard protocol for cutting micro-sections and collecting high-resolution images proposed by von Arx *et al.* (2016). From each disc, we extracted radial wood

samples from opposite radii (Fig. S2) and produced 10-15 µm thick cross-sections using a rotary microtome (Leica RM2245, Leica Biosystems, Nussloch, Germany). In addition, for ray parenchyma quantification (see below), we cut three tangential sections from each wood sample within the annual rings formed in 2000, 2006 and 2011 to include years from all the different treatment combinations (Table 1). All sections were stained with safranin and astrablue and permanently fixed with Eukitt (BiOptica, Milan, Italy). Overlapping images of the cross-sections and tangential sections were captured at 100× magnification using a light microscope connected to a digital camera (Nikon Eclipse 80i,Nikon, Tokyo, Japan), and then stitched using PTGui (version 8.3.3, New House Internet Services B.V., Rotterdam, NL) to obtain high-resolution images (2.07 pixels/µm). Image analysis was performed with ROXAS version 2.1 (von Arx & Dietz 2005; von Arx & Carrer 2014) which provided ring width and several measurements of cell anatomical features such as tracheid lumen area and wall thickness from cross-sections (Prendin *et al.* 2017) and ray cell lumen area from tangential sections (see Fig. S3). In total, we produced annual anatomical trait values (see below) for c. 1300 rings based on measurements from >5 million tracheids. Compression wood rings were excluded from analysis.

Functional anatomical traits

For each annual ring of each disc, we derived xylem functional traits using the aforementioned basic anatomical measurements (Table 2). For the functional traits calculated on earlywood (EW) and latewood (LW) tissue, tracheids were assigned to each tissue based on Mork's index, i.e. the ratio between twice the double-cell wall thickness and the lumen diameter (Denne 1988). As a proxy for the hydraulic efficiency, we used the mean hydraulic diameter (*Dh*), i.e. the lumen diameter corresponding to the mean hydraulic conductivity among all tracheids (Sperry *et al.* 1994; Kolb & Sperry 1999). *Dh* was calculated separately for the above-ground (Dh_{STEM}) and below-ground (Dh_{ROOT}) organs to account for their different demands and constraints. In addition, we calculated *Dh* of the apex (Dh_{APEX}) due to its importance as the starting point for the axial tracheid widening. As an

255 indicator of the hydraulic safety from cell implosion, we used the 5th percentile of cell wall
256 reinforcement ($(t/b)^2$) (Hacke *et al.* 2001) (corresponding to the widest and most implosion-prone
257 tracheids), where t is the double-cell wall thickness and b is the lumen diameter of the tracheid
258 measured perpendicularly to the double-cell wall thickness. This produced two values per tracheid,
259 one with radial and one with tangential orientation of lumen diameter. For each tracheid, the smaller
260 of the two values was used to better reflect the risk of cell implosion. The mechanical support function
261 of the xylem was estimated by the mean cell wall thickness of latewood tracheids (CWT_{LW}), as well
262 as by the percentage of latewood. As a proxy for the metabolically active tissue, we considered the
263 percent area of ray parenchyma (*PERPAR*; von Arx et al. 2015), measured here as the sum of ray cell
264 lumen areas divided by the tangential section area (c. 5 mm^2, see Fig. S3). To account for the different
265 demands and constraints, above- and below-ground organs we calculated separately as $PERPAR_{STEM}$
266 and $PERPAR_{ROOT}$.
267
268 Additionally, we devised the 'hydraulic carbon use efficiency' index (*HCUE*) to express the hydraulic
269 return for a given carbon investment. *HCUE* was calculated for each ring as the ratio of the
270 accumulated theoretical conductance of all tracheids (*Kh* according to Poiseuille's law, Tyree &
271 Ewers 1991) to the accumulated wall area of all tracheids within the ring (CWA_{RING}). Finally, as a
272 proxy for growth, the ring area (*RA*) of each ring (c. 1300) was estimated based on the ROXAS ring
273 width measurements assuming a circular stem cross-section.
274
275 **Estimation of axial scaling and treatment effects**
276
277 For each functional tracheid trait (*Dh*, $(t/b)^2$, CWT_{LW}), we fitted linear, power and exponential
278 functions to identify which function best described the axial scaling. Fitting was performed only for
279 stem annual rings from trees that were not subject to any treatment (treatments A_{2001} and A, see Table
280 1) to avoid potential confounding treatment effects. In addition, to check for ontogenetic trends, we

281 computed the scaling exponents ('slope') throughout the life of each tree using a model type II
282 regression analysis with the reduced major axis (RMA) protocol in the lmodel2 R package (Legendre
283 2014). We based this analysis on data from a moving window of three neighbouring tree rings to
284 increase the number of axial points, which then did not allow us to additionally check for interactions
285 between ontogeny and treatments. This analysis could only be performed with data from 2001 to
286 2012, thus not covering the first c. 30 years of tree growth. Similarly, we established the relationships
287 among the functional traits (*Dh*, $(t/b)^2$, CWT_{LW} and *PERPAR*) in terms of axial scaling and trait
288 covariance by identifying the function (linear, power or exponential) that provided the highest R^2.
289 The initial exploration of the covariance of the functional traits with the overall dataset revealed that
290 the power functions fit best (data not shown). The covariance of functional traits in tree rings of
291 different cambial age was then assessed with the best fitting function and evaluated for trends in the
292 pairwise relationships during ontogeny and treatments. In addition, we tested the relationship between
293 each functional trait (*Dh*, $(t/b)^2$, CWT_{LW} and *PERPAR*) and each growth parameter *ΔH and RAI* (see
294 Table 2).
295
296 Treatment effects on the axial patterns were tested using linear mixed-effects models fitted with
297 restricted maximum likelihood (REML). We established a model for each response variable (Dh_{ROOT},
298 $(t/b)^2$, CWT_{LW}, *PERPAR and HCUE),* where distance from the apex (*L*), treatment combinations (see
299 Table 1) and their interactions were included as fixed effects, and tree identity and disc height along
300 the tree axis as random factors in all initial models, reflecting the experimental design and the sample
301 collection. Response variables were $\log_{10}$-transformed to comply with assumptions of normality and
302 homoscedasticity (Zar 1999). For the Dh_{STEM} model, we additionally included Dh_{APEX} as a fixed effect
303 to account for its known strong influence on Dh_{STEM} (Petit *et al.* 2011). For this model, we only
304 considered annual rings for which apical data (defined as ≤1 cm from tree top) were available. The
305 best model was chosen based on AICc using the maximum likelihood method (Zuur *et al.* 2009).
306 When several models showed similar AICc values (ΔAICc <2, Burnham & Anderson 2002), they

were refitted with the REML method to obtain estimates and significance values of effects, and the simplest model with significant fixed effects was chosen as the 'optimal' model. The significance of the fixed effects was tested with F tests (Pinheiro & Bates 2000). When the target functional trait did not exhibit a significant axial trend, the difference between treatment combinations was tested with Tukey's Honest Significance test based on ANOVA. All analyses were performed using R (version 3.1.1; R Development Core Team 2014), and linear mixed-effects models were run using the lme4 (Bates *et al.* 2015) and MuMIn packages (Barton & Barton 2013).

RESULTS

Axial scaling of xylem trait

The analysis of the functional trait variability along the whole tree axis using different parametric functions (Fig. 1a-d) revealed that the power function provided the best fit to the data, with R^2 values ranging from 0.81 (*Dh*) to 0.16 (CWT_{LW}) (Table 3). However, for CWT_{LW} the power function performed only slightly better than the linear and exponential ones. Tracheid hydraulic diameter (*Dh*) increased continuously down the stem and further along the roots (see also the axial profile for the tree ring of 2011 for tree E3L1 shown in Fig. 1a). This widening pattern was narrowly confined for the stem, thus indicating only small differences among individuals and no significant changes throughout ontogeny (P=0.81, Fig. 2a). For each year of growth, *Dh* in the roots was larger than in the stem, generally increased with L at faster rates than in the stem, and showed more variation in the data (R^2=*0.10*) (Fig. 1a).

The 5th percentile of cell wall reinforcement $(t/b)^2$ decreased continuously from the stem apex to the stem base and further below ground along the roots. In the stem, L explained 46% of the total variance in $(t/b)^2$ (Table 3), while in the roots this relationship was not significant (P=0.31) (Fig. 1b). Additionally, the scaling exponent (b) of the relationship of $(t/b)^2$ vs. distance from the apex (L)

progressively decreased with tree age (R^2=0.48, P<0.001, Fig. 2b). The cell wall thickness of the latewood tracheids (CWT_{LW}) increased continuously from the stem apex to the base and further along the roots (Fig. 1c). The inter-annual variability was substantial in this trait, as shown by the low R^2 of 0.16 for the stem (Table 3) and the non-significant relationship for the roots (P=0.90). Furthermore, the scaling exponent b of the power function relating CWT_{LW} to L progressively increased with tree age (R^2=0.86, P<0.001, Fig. 2c). However, this ontogenetic trend was only significant when a power function was used but not when linear or exponential fitting was applied (P=0.71 and P=0.11, respectively). The percentage of latewood did not show an axial trend (Fig. S4a) and was significantly related to CWT_{LW} (R^2=0.38 and R^2=0.09, P<0.001, for stem and root, respectively; Fig. S4b). The experimental design did not allow us to additionally test for treatment effects on the ontogenetic trend. The percent area of ray parenchyma (*PERPAR*) did not change significantly with distance from the apex in the stem (P=0.53) and root (P=0.83) (Fig. 1d).

Treatment effects on axial trait scaling

The linear mixed-effect models used to test for the importance of treatments on the axial scaling of Dh_{STEM} did not reveal any significant effects (Table 4, Fig. 1e). Along the roots, *Dh* was in general wider before 2001, whereas all treatment combinations except EC (elevated CO_2) showed a significant overall reduction in Dh_{ROOT} (Table 4, Fig. 1f). Treatment effects on $(t/b)^2$ were found for the combination of soil warming and elevated CO_2 (ECSW), also after CO_2 fumigation ceased in 2009 (PECSW), as shown by a steeper increase in $(t/b)^2$ with increasing distance from the apex. The model results for CWT_{LW} were analogous to those for $(t/b)^2$ (Table 4, Fig. 1g). Similarly, the axial scaling of *HCUE* was influenced by the same treatment combinations as $(t/b)^2$ and CWT_{LW}, but with inversed relationships. In addition, *HCUE* for A_{2001} was smaller at the stem apex (i.e., smaller intercept a) but increased along the stem at a faster rate (larger b) than for the same trees after they had grown taller, irrespective of treatments. *PERPAR* showed no significant axial variation, and the

359 one-way ANOVA performed instead to test for treatment effects revealed that soil warming (SW)
360 had a significant negative effect on the production of ray parenchyma (P=0.035) but no other
361 treatment effects were significant.
362
363 **Trait trade-offs during ontogeny and under treatments**
364
365 Pairwise comparisons between functional traits using a power function revealed a significant trade-
366 off between proxies of hydraulic efficiency and safety (Dh vs. $(t/b)^2$) (Fig. 3), which seems partly due
367 to their link through tracheid diameter. The slope b of the relationship $Log_{10}Dh = Log_{10}$ a + b·Log_{10}
368 $(t/b)^2$ became less negative with increasing cambial age in stems and roots, respectively; Fig. 3),
369 independent from treatment with the exception of *PECSW* in the stem, which showed no ontogenetic
370 trend (P>0.05). Furthermore, stem hydraulic efficiency (Dh) was negatively linked (b-values pre-
371 dominantly <0) to mechanical support (CWT_{LW}) with no significant change related to cambial age or
372 treatment (Fig. 3). In contrast, $(t/b)^2$ and CWT_{LW} were unrelated in the stem (slope b scattered around
373 0) and positively related in the roots (b-values mostly >0) with no ontogenetic trend or treatment
374 effect (Fig. 3). The pairwise relationship of *PERPAR* with the other functional traits was only assessed
375 globally because of the reduced dataset (only data for 2000, 2006 and 2011) and revealed no
376 significant relationship (Fig. S5).
377
378 **Hydraulic efficiency: costs and effect on growth**
379
380 The analyses of *HCUE*, the ratio between hydraulic conductance and structural carbon costs,
381 indicated that, per unit of conductance, construction costs increase with height along the stem (Fig.
382 4, Table 3).
383

384 Of all the considered functional traits, only the hydraulic diameter at the stem apex (Dh_{APEX}) had a
385 significant effect (P<0.001) on growth (Fig. 5; other data not shown). Indeed, Dh_{APEX} explained 31%
386 and 36% of the total variance in ΔH and RAI, respectively, independent from ontogeny and treatment
387 (P>0.05).
388
389 **DISCUSSION**
390
391 **Axial scaling of functional traits is linked to biophysical principles**
392
393 Our description of xylem anatomical traits showed characteristic axial scaling that can be attributed
394 to different biophysical principles. As expected, the hydraulic efficiency (Dh) scaled along the stem
395 following a power function with a scaling exponent (b=0.17) very similar to values reported in other
396 studies (Petit *et al.* 2011; Anfodillo *et al.* 2013). This supports the remarkable universality of the axial
397 conduit widening in vascular plants (West *et al.* 1999; Anfodillo *et al.* 2006; Olson *et al.* 2014) here
398 demonstrated for the first time for trees subject to experimental manipulation of environmental
399 conditions. Furthermore, in all trees and under all treatment combinations, xylem tracheids in the
400 roots were wider than along the stem, in agreement with previous studies (McElrone *et al.* 2004; Petit,
401 Anfodillo & De Zan 2009; Petit *et al.* 2010). This strict axial configuration represents a biophysical
402 optimization to buffer the increasing hydraulic resistance due to a longer path length as trees grow
403 taller (West *et al.* 1999; Petit & Anfodillo 2009). Instead, the cell wall reinforcement $(t/b)^2$ of the
404 earlywood increased towards the apex, i.e. in parallel with the decrease in the water potential towards
405 the apex (Domec, Pruyn & Gartner 2005). This is in line with previous findings showing a decrease
406 with tree age and increase with height (Domec *et al.* 2009). The latewood cell wall thickness (CWT_{LW})
407 increased from stem apex to base (Fig. 1c), thus indicating an increasing need for mechanical support
408 by the latewood along the stem. Such mechanically stronger latewood cells might be required to
409 compensate for the decreasing contribution of the earlywood to ring-level mechanical support

410 towards the stem base as earlywood tracheid diameter increases. However, this increase was relatively
411 small compared to, for example, the increase in accumulated biomass to the power of three to four
412 when moving down the stem, as reconstructed for an individual of *Abies procera* (King 2011), thus
413 suggesting a non-linear relationship between cell wall thickness and the mechanical support provided.
414
415 In contrast to the other functional tracheid traits, we did not find a consistent or clearly defined axial
416 trend for the percent area of ray parenchyma (*PERPAR*) as expected. Indeed an increase in ray size
417 with age and distance from the stem apex, following the increase in tracheid size, would be expected
418 (Lev-Yadun & Aloni 1995). The variability along the stem axis was very large both between and
419 within trees (ranging from 0.12 to 2.55%). This finding confirms previous observations that the ray
420 proportion of conifers varies widely, both among individuals (Fonti *et al.* 2015; von Arx et al. 2017)
421 and within the stem (DeSmidt 1922; Baker, Spicer & Gartner 2000; von Arx *et al.* 2015), with only
422 a relatively weak influence of environmental conditions (Esteban *et al.* 2012; Olano *et al.* 2013)
423 and/or functional needs such as storage space requirements (von Arx *et al.*, 2017).
424
425 Generally, the trends observed in the roots were consistent with those observed in the stem but were
426 much weaker, probably because roots are buffered against much of the above-ground environmental
427 variability and also more responsive to soil geomorphic processes (Gärtner, Schweingruber & Dikau
428 2001). This increased variability might be because, compared to stems, roots have additional
429 functions (e.g., flexibility, stiffness, anchorage) within a less homogeneous medium (different soil
430 texture and depth) (Gärtner, Schweingruber & Dikau 2001).
431
432 **Hydraulic efficiency shows no ontogenetic trend but a trade-off with hydraulic safety**
433
434 During ontogeny, adjustments of the xylem structure are necessary to meet the changing functional
435 needs as tree size increases. Despite these expected modifications, the power fitting observed for

436 hydraulic efficiency (*Dh*) appeared to be stable and independent from the ontogenetic tree
437 development, suggesting strong biophysical control over the axial design of hydraulic efficiency. In
438 contrast, hydraulic safety ($(t/b)^2$) showed a slight change in the axial scaling, which suggests a
439 decrease in safety with increasing tree size. A possible explanation for this ontogenetic trend is that
440 larger trees have a deeper root system with better access to soil water (Rosner 2013). Similarly, at
441 least when using power fitting, the axial scaling of the mechanical support (CWT_{LW}) changed in a
442 way that suggested an increase during the course of a tree's life for a given distance from the apex.
443 This may reflect size-related changes in tree architecture, since many trees invest increasingly into
444 lateral structures as they grow taller, which requires stronger wood to support it (King, 2011).
445
446 Limited resources to form wood and differing biophysical constraints inherently imply trade-offs
447 between the xylem functional needs, as demonstrated by the competing axial structural adjustments
448 observed in our study (Fig. 2). Specifically, and as hypothesized, we confirmed the presence of a
449 trade-off between hydraulic efficiency and safety (Sperry, Meinzer & McCulloh 2008; Bouche *et al.*
450 2014; Hacke 2015; Gleason *et al.* 2016). In addition, hydraulic efficiency was negatively related to
451 mechanical stability. The observed hydraulic efficiency vs. safety trade-off is related to the fact that
452 tracheids with narrow lumina are less efficient in transporting water but more resistant to implosion
453 and xylem cavitation (Gleason *et al.* 2016). Our results suggest that this relationship changes along
454 the stem axis in order to prioritize safety towards the stem apex and efficiency toward the stem base
455 (Fig. 2). This result is supported by the fact that the construction costs for the hydraulic system
456 (*HCUE* , i.e. the hydraulic conductance per unit of cell wall area) were higher towards the stem apex
457 (Fig. 4, Table 3). This could be explained by the importance of an undamaged apex to sustain height
458 growth and compete with neighbouring trees, particularly in a conifer with clear apical dominance
459 such as *L. decidua*.
460
461 **Environmental conditions have a differential impact on functional traits**

462

463 Previous studies suggested that *L. decidua* responded more to elevated CO_2 than soil warming (Handa
464 *et al.* 2006; Dawes *et al.* 2011, 2015), e.g. by increased above-ground growth (Dawes *et al.* 2011,
465 2015), including greater leaf canopy (Streit et al., 2014) and increased accumulation of non-structural
466 carbohydrates (Hatterschwiler et al., 2002, Handa et al., 2005). Our results suggest that soil warming
467 and elevated CO_2 did not strongly influence the scaling of the analysed functional traits along the
468 stem (Table 3). As hypothesized, effects of environmental conditions emerged only in the functional
469 traits that did not show a very strong biophysical determination, for example the mean hydraulic
470 diameter in the roots (Dh_{ROOT}) and the percent area of ray parenchyma (*PERPAR*). Specifically, the
471 soil warming treatment had a local effect restricted to root xylem anatomy. The significant decrease
472 in Dh_{ROOT} under soil warming implies reduced overall root conductance because no significant
473 compensating increase in root biomass was observed (Dawes *et al.* 2015). However, when
474 considering that a 4 °C increase in water temperature lowers viscosity and thus hydraulic resistance
475 by c. 12% according to the Hagen-Poiseuille equation (Tyree & Zimmermann 2002), the observed
476 increase in hydraulic resistance due to slightly smaller Dh_{ROOT} is in roughly the same range, thus
477 resulting in a net effect of zero. In any case, due to the comparably minimal hydraulic resistance of
478 the wide root tracheids, such a small decrease in lumen size has almost no effect on overall pathway
479 length resistance and therefore likely no functional relevance for whole plant conductance,
480 transpiration and photosynthesis. Soil warming also reduced $PERPAR_{STEM}$ but not $PERPAR_{ROOT}$.
481 However, treeline trees are usually relatively rich in NSCs and starch reserves (Hoch & Körner 2012),
482 and the different warming effects on *PERPAR* in the stem and roots may reflect an osmotic adjustment
483 of the root-to-leaf gradient of water potential that effectively influences the translocation of sugars
484 within the plant (Hölttä *et al.* 2006; Dawes *et al.* 2014).

485

486 Furthermore, our results showed a weak increase in $(t/b)^2$ and CWT_{LW} with increasing distance from
487 apex (L) under ECSW and PECSW, meaning that trees profited from the larger amount of

488 photosynthates available under elevated CO_2, by having a greater needle biomass (Dawes *et al.* 2015)
489 and by increasing the mechanical stability of the trunk (Fig. 1f, Fig. 1g). At the same time, the
490 significantly lower values of $(t/b)^2$ and CWT_{LW} close to the stem apex under CO_2 enrichment could
491 explain the increase in freezing sensitivity of trees exposed to elevated CO_2, particularly in taller
492 trees, as previously observed for the period 2005-2010 (Martin *et al.* 2010; Rixen *et al.* 2012).
493
494 **Greater mean hydraulic diameter at the apex promotes growth**
495
496 The observed within-tree variability of anatomical traits and its influence on tree functioning lead to
497 the obvious question about the relevance for growth. Of all the functional traits analysed in this
498 respect, only the mean hydraulic diameter at the stem apex (Dh_{APEX}) was important, explaining 31%
499 and 36% of the variability in stem elongation and ring area at the stem base, respectively (Fig. 5).
500 This result highlights the importance of hydraulic efficiency for growth. More specifically, the finding
501 that Dh_{APEX}, and not Dh_{STEM} or Dh_{ROOT}, was significant is remarkable. Indeed, the apex is a hydraulic
502 bottleneck restricting growth (Petit et al. 2011; West *et al.* 1999; Petit & Anfodillo 2009), and
503 previous studies showed that Dh_{APEX} increases slightly as trees grow taller, presumably to counteract
504 the concomitant increase in water tension accompanying height growth (Petit, Anfodillo &
505 Mencuccini 2008; Olson *et al.* 2014). Our results are thus in line with these studies and support the
506 view that an increase in the conductivity of the stem apex releases the hydraulic constraints on water
507 transport, thus favouring gas exchange and ultimately growth (Petit *et al.* 2011).
508
509 **Conclusions**
510
511 In this study we quantified xylem anatomical traits in tree rings along the stem and root axis and
512 derived corresponding xylem functions to identify priorities and trade-offs and to determine if
513 ontogeny or experimental manipulation of CO_2 and temperature influence these relationships. The

514 strong biophysical constraints resulted in a narrowly confined axial pattern of *Dh*, suggesting a
515 prioritization of hydraulic efficiency over other xylem functions (hydraulic safety, mechanical
516 support, metabolic functions). Likewise, at the apex, a tree's hydraulic bottleneck, a small increase in
517 *Dh* significantly enhances water transport, thus fuelling carbon assimilation supporting growth. The
518 higher variability of the other functional traits potentially indicates a greater ability or need to respond
519 to the environment and ontogenetic development. Moreover, our findings indicate that the overall
520 architectural design of the tree requires a certain priority towards hydraulic safety towards the stem
521 apex, while hydraulic efficiency and mechanical support gain progressively more importance towards
522 the stem base. In conclusion, our study suggests that prioritized xylem functional traits show a very
523 strong biophysical determination, while subordinate traits respond more plastically to intrinsic and
524 extrinsic factors.
525

526 ## Authors' Contributions

527

528 All authors planned and designed the research, and CR, MAD and PF conducted the fieldwork. ALP
529 collected the data. ALP, GP, PF and GvA analysed the data. ALP led the manuscript drafting with
530 contributions from GP, PF and GvA. All authors discussed, revised and approved the manuscript.
531

532 ## Acknowledgements

533

534 We thank S. Hättenschwiler for initiating and F. Hagedorn for running the 12-year CO_2 enrichment
535 and soil warming experiment, as well as many colleagues at the WSL and SLF for assistance with
536 field work and technical support. We acknowledge S. Lechthaler in particular for helping with
537 measurements on tangential sections. Major funding sources for this treeline experiment included the
538 Swiss National Science Foundation from 2001-2005 (grant 31-061428.00 to S. Hättenschwiler) and

from 2007-2010 (grant 315200-116861 to CR); the Velux Foundation from 2007 to 2012 (grant 371 to F. Hagedorn); and the WSL from 2012 to 2016 (grant to CR and MAD). This particular study was supported by the COST Action F1106 “Studying Tree Responses to extreme Events”. GvA was supported by grants from the Swiss State Secretariat for Education, Research and Innovation SERI (SBFI C14.0104 and C12.0100).

Data Accessibility

Data are deposited in the Dryad Digital Repository http://dx.doi.org/10.5061/dryad.k6516 (Prendin et al., 2017b)

553 ## References

554 Anderegg, W.R.L., Plavcová, L., Anderegg, L.D.L., Hacke, U.G., Berry, J.A. & Field, C.B. (2013)
555 Drought's legacy: multiyear hydraulic deterioration underlies widespread aspen forest die-off
556 and portends increased future risk. *Global Change Biology*, **19**, 1188–1196.

557 Anfodillo, T., Carraro, V., Carrer, M., Fior, C. & Rossi, S. (2006) Convergent tapering of xylem
558 conduits in different woody species. *New Phytologist*, **169**, 279–290.

559 Anfodillo, T., Petit, G. & Crivellaro, A. (2013) Axial conduit widening in woody species: a still
560 neglected anatomical pattern. *IAWA Journal*, **34**, 352–364.

561 von Arx, G., Arzac, A., Fonti, P., Frank, D., Zweifel, R., Rigling, A., Galiano, L., Gessler, A. &
562 Olano, M. (2017) Responses of sapwood ray parenchyma and non-structural carbohydrates of
563 Pinus sylvestris to drought and long-term irrigation. *Functional Ecology*, **31**, 1371–1382.

564 von Arx, G., Arzac, A., Olano, J.M. & Fonti, P. (2015) Assessing conifer ray parenchyma for
565 ecological studies: pitfalls and guidelines. *Frontiers in Plant Science*, **6**, 1016.

566 von Arx, G. & Carrer, M. (2014) ROXAS – A new tool to build centuries-long tracheid-lumen
567 chronologies in conifers. *Dendrochronologia*, **32**, 290–293.

568 von Arx, G., Crivellaro, A., Prendin, A.L., Čufar, K. & Carrer, M. (2016) Quantitative wood
569 anatomy—practical guidelines. *Frontiers in Plant Science*, **7**, 781.

570 von Arx, G. & Dietz, H. (2005) Automated image analysis of annual rings in the roots of perennial
571 forbs. *International Journal of Plant Sciences*, **166**, 723–732.

572 Baker, D.C., Spicer, R. & Gartner, B.L. (2000) Distribution and vitality of xylem rays in relation to
573 tree leaf area in Douglas-fir. *IAWA Journal*, **21**, 389–401.

574 Bannan, M.W. (1937) Observations on the distribution of xylem-ray tissue in conifers. *Annals of*
575 *Botany*, **1**, 717–726.

576 Barbeito, I., Dawes, M. a, Rixen, C., Senn, J. & Bebi, P. (2012) Factors driving mortality and growth
577 at treeline: a 30-year experiment of 92 000 conifers. *Ecology*, **93**, 389–401.

578 Barton, K. & Barton, M.K. (2013) MuMIn: multi-model interference. R Package version 1.9.5.
579 Available at http://r-forge.r-project.org/projects/mumin/10/6/2013
580 Bates, D., Mächler, M., Bolker, B. & Walker, S. (2015) Fitting linear mixed-effects models using
581 lme4. *Journal of Statistical Software*, **67**, arXiv:1406.5823.
582 Beeckman, H. (2016) Wood anatomy and trait-based ecology. *IAWA Journal*, **37**, 127–151.
583 Bittencourt, P.R.L., Pereira, L. & Oliveira, R.S. (2016) On xylem hydraulic efficiencies, wood space-
584 use and the safety-efficiency tradeoff. *New Phytologist*, **211**, 1152–1155.
585 Björklund, J., Seftigen, K., Schweingruber, F., Fonti, P., von Arx, G., Bryukhanova, M.V., Cuny,
586 H.E., Carrer, M., Castagneri, D. & Frank, D.C. (2017) Cell size and wall dimensions drive
587 distinct variability of earlywood and latewood density in Northern Hemisphere conifers. *New*
588 *Phytologist*, DOI: 10.1111/nph.14639
589 Bouche, P.S., Larter, M., Domec, J.C., Burlett, R., Gasson, P., Jansen, S. & Delzon, S. (2014) A broad
590 survey of hydraulic and mechanical safety in the xylem of conifers. *Journal of Experimental*
591 *Botany*, **65**, 4419–4431.
592 Brodersen, C.R. & McElrone, A.J. (2013) Maintenance of xylem network transport capacity: a review
593 of embolism repair in vascular plants. *Frontiers in Plant Science*, **4**, 1–11.
594 Burnham, K.P. & Anderson, D.R. (2002) *Model selection and multimodel inference a practical*
595 *information-theoretic approach (2nd Edition)*. Ecological Modeling. Springer-Verlag New York,
596 Inc.
597 Choat, B. (2013) Predicting thresholds of drought-induced mortality in woody plant species. *Tree*
598 *Physiology*, **33**, 669–671.
599 Dawes, M.A., Hättenschwiler, S., Bebi, P., Hagedorn, F., Handa, I.T., Körner, C. & Rixen, C. (2011)
600 Species-specific tree growth responses to 9 years of CO_2 enrichment at the alpine treeline.
601 *Journal of Ecology*, **99**: 382-394.
602 Dawes, M.A., Philipson, C.D., Fonti, P., Bebi, P., Hättenschwiler, S., Hagedorn, F. & Rixen, C.
603 (2015) Soil warming and CO_2 enrichment induce biomass shifts in alpine tree line vegetation.

Global Change Biology, **21**, 2005–2021.

Dawes, M.A., Zweifel, R., Dawes, N., Rixen, C. & Hagedorn, F. (2014) CO_2 enrichment alters diurnal stem radius fluctuations of 36-yr-old *Larix decidua* growing at the alpine tree line. *New Phytologist*, **202**, 1237–1248.

Denne, M.P. (1988) Definition of latewood according to Mork (1928). *IAWA Journal*, **10**, 59–62.

DeSmidt, W.J. (1922) Studies of the distribution and volume of the wood rays in slippery elm (*Ulmus Fulva* Michx.). *Journal of Forestry*, **20**, 352–362.

Domec, J.-C. & Gartner, B.L. (2002) How do water transport and water storage differ in coniferous earlywood and latewood? *Journal of Experimental Botany*, **53**, 2369–2379.

Domec, J.C., Pruyn, M.L. & Gartner, B.L. (2005) Axial and radial profiles in conductivities, water storage and native embolism in trunks of young and old-growth ponderosa pine trees. *Plant, Cell & Environment*, **28**, 1103–1113.

Domec, J.-C., Lachenbruch, B., Meinzer, F.C., Woodruff, D.R., Warren, J.M. & McCulloh, K.A. (2008) Maximum height in a conifer is associated with conflicting requirements for xylem design. *Proceedings of the National Academy of Sciences of the United States of America*, **105**, 12069–12074.

Domec, J.-C., Warren, J.M., Meinzer, F.C. & Lachenbruch, B. (2009) Safety factors for xylem failure by implosion and air-seeding within roots, trunks and branches of young and old conifer trees. *IAWA Journal*, **30**, 101–120.

Esteban, L.G., Martín, J.A., de Palacios, P. & Fernández, F.G. (2012) Influence of region of provenance and climate factors on wood anatomical traits of *Pinus nigra* Arn. subsp. *salzmannii*. *European Journal of Forest Research*, **131**, 633–645.

Fatichi, S., Leuzinger, S. & Körner, C. (2014) Moving beyond photosynthesis: from carbon source to sink-driven vegetation modeling. *New Phytologist*, **201**, 1086–1095.

Fatichi, S., Rimkus, S., Burlando, P., Bordoy, R. & Molnar, P. (2013) Elevational dependence of climate change impacts on water resources in an Alpine catchment. *Hydrology and Earth System*

630 *Sciences Discussions*, **10**, 3743–3794.
631 Finto, A., Schimleck, L. & Daniels, R. (2012) A comparison of earlywood-latewood demarcation
632 methods–A case study in loblolly pine. *IAWA journal*, **33**, 187–195.
633 Fonti, P., von Arx, G., García-González, I., Eilmann, B., Sass-Klaassen, U., Gärtner, H. & Eckstein,
634 D. (2010) Studying global change through investigation of the plastic responses of xylem
635 anatomy in tree rings. *New Phytologist*, **185**, 42–53.
636 Fonti, P. & Jansen, S. (2012) Xylem plasticity in response to climate. *New Phytologist*, **195**, 734–
637 736.
638 Fonti, P., Tabakova, M.A., Kirdyanov, A.V., Bryukhanova, M.V. & von Arx, G. (2015) Variability
639 of ray anatomy of *Larix gmelinii* along a forest productivity gradient in Siberia. *Trees*, **29**, 1165–
640 1175.
641 Gartner, B.L., Baker, D.C. & Spicer, R. (2000) Distribution and vitality of xylem rays in relation to
642 tree leaf area in Douglas-fir. *IAWA Journal*, **21**, 389–401.
643 Gärtner, H., Schweingruber, F.H. & Dikau, R. (2001) Determination of erosion rates by analyzing
644 structural changes in the growth pattern of exposed roots. *Dendrochronologia*, **19**, 81–91.
645 Gleason, S.M., Westoby, M., Jansen, S., Choat, B., Hacke, U.G., Pratt, R.B., Bhaskar, R., Brodribb,
646 T.J., Bucci, S.J., Cao, K., Fan, Z., Feild, T.S., Jacobsen, A.L., Johnson, D.M., Domec, J.,
647 Mitchell, P.J., Morris, H., Nardini, A., Pittermann, J., Schreiber, S.G., Sperry, J.S., Wright, I.J.
648 & Zanne, A.E. (2016) Weak tradeoff between xylem safety and xylem- specific hydraulic
649 efficiency across the world's woody plant species. *New Phytologist*, **209**, 123–136.
650 Hacke, U. (2015) *Functional and Ecological Xylem Anatomy* (ed U Hacke). Springer International
651 Publishing, Cham
652 Hacke, U.G., Sperry, J.S., Pockman, W.T., Davis, S.D. & McCulloh, K.A. (2001) Trends in wood
653 density and structure are linked to prevention of xylem implosion by negative pressure.
654 *Oecologia*, **126**, 457–461.
655 Hagedorn, F., Martin, M.A., Rixen, C., Rusch, S., Bebi, P., Zürcher, A., Siegwolf, R.T.W., Wipf, S.,

656 Escape, C., Roy, J. & Hättenschwiler, S. (2010) Short-term responses of ecosystem carbon
657 fluxes to experimental soil warming at the Swiss alpine treeline. *Biogeochemistry*, **97**, 7–19.
658 Handa, I.T., Körner, C. & Hättenschwiler, S. (2005) A test of the treeline carbon limitation hypotesis
659 by in situ CO_2 enrichment and defoliation. *Ecology, Functional*, **86**, 1288–1300.
660 Handa, I.T., Körner, C. & Hättenschwiler, S. (2006) Conifer stem growth at the altitudinal treeline in
661 response to four years of CO_2 enrichment. *Global Change Biology*, **12**, 2417–2430.
662 Harsch, M.A., Hulme, P.E., McGlone, M.S. & Duncan, R.P. (2009) Are treelines advancing? A global
663 meta-analysis of treeline response to climate warming. *Ecology Letters*, **12**, 1040–1049.
664 Hättenschwiler, S., Handa, I.T., Egli, L., Asshoff, R., Ammann, W. & Körner, C. (2002) Atmospheric
665 CO2 enrichment of alpine treeline conifers. *New Phytologist*, **156**, 363–375.
666 Hoch, G. & Körner, C. (2012) Global patterns of mobile carbon stores in trees at the high-elevation
667 tree line. *Global Ecology and Biogeography*, **21**, 861–871.
668 Hölttä, T., Vesala, T., Sevanto, S., Perämäki, M. & Nikinmaa, E. (2006) Modeling xylem and phloem
669 water flows in trees according to cohesion theory and Münch hypothesis. *Trees*, **20**, 67–78.
670 Jyske, T., Mäkinen, H. & Saranpää, P. (2008) Wood density within Norway Spruce stems. *Silva*
671 *Fennica*, **42**, 439–455.
672 King, D.A. (2011) Size-related changes in tree proportions and their potential influence on the course
673 of height growth. *Tree Physiology*, Tree Physiology (eds F.C. Meinzer, B. Lachenbruch & T.E.
674 Dawson), pp. 165–191. Springer Netherlands, Dordrecht.
675 Koch, G.W., Sillett, S.C., Jennings, G.M. & Davis, S.D. (2004) The limits to tree height. *Nature*, **428**,
676 851–854.
677 Kolb, K.J. & Sperry, J.S. (1999) Transport constraints on water use by the Great Basin shrub,
678 *Artemisia tridentata*. *Plant, Cell & Environment*, **22**, 925–935.
679 Körner, C. (2012) *Alpine Treelines*. Springer Basel, Basel.
680 Koubaa, A., Zhang, S.Y.T. & Makni, S. (2002) Defining the transition from earlywood to latewood

681 in black spruce based on intra-ring wood density profiles from X-ray densitometry. *Annals of*
682 *Forest Science*, **59**, 511–518.
683 Lachenbruch, B. & McCulloh, K.A. (2014) Traits, properties, and performance: how woody plants
684 combine hydraulic and mechanical functions in a cell, tissue, or whole plant. *New Phytologist*,
685 **204**, 747–764.
686 Larson, P.R. (1963) Stem form development of forest trees. *Forest science*, **9**, a0001–a0001.
687 Lazzarin, M., Crivellaro, A., Williams, C.B., Dawson, T.E., Mozzi, G. & Anfodillo, T. (2016)
688 Tracheid and pit anatomy vary in tandem in a tall *Sequoiadendron giganteum* tree. *IAWA*
689 *Journal*, **37**, 172–185.
690 Legendre, P. (2014) lmodel2: Model II Regression. Rpackage version 1.7-2. Available at:
691 http://CRAN.R-project.org/package=lmodel2.
692 Lev-Yadun, S. & Aloni, R. (1995) Differentiation of the ray system in woody plants. *The Botanical*
693 *Review*, **61**, 45–84.
694 Lintunen, A., Paljakka, T., Jyske, T., Peltoniemi, M., Sterck, F., von Arx, G., Cochard, H., Copini,
695 P., Caldeira, M.C., Delzon, S., Gebauer, R., Grönlund, L., Kiorapostolou, N., Lechthaler, S.,
696 Lobo-do-Vale, R., Peters, R.L., Petit, G., Prendin, A.L., Salmon, Y., Steppe, K., Urban, J., Roig
697 Juan, S., Robert, E.M.R. & Hölttä, T. (2016) Osmolality and non-structural carbohydrate
698 composition in the secondary phloem of trees across a latitudinal gradient in Europe. *Frontiers*
699 *in Plant Science*, **7**, 726.
700 Lundgren, C. (2004) Cell wall thickness and tangential and radial cell diameter of fertilized and
701 irrigated Norway spruce. *Silva Fennica*, **38**, 95–106.
702 Martin, M., Gavazov, K., Körner, C., Hättenschwiler, S. & Rixen, C. (2010) Reduced early growing
703 season freezing resistance in alpine treeline plants under elevated atmospheric CO_2. *Global*
704 *Change Biology*, **16**, 1057–1070.
705 Mcculloh, K.A., Johnson, D.M., Meinzer, F.C. & Woodruff, D.R. (2014) The dynamic pipeline :
706 hydraulic capacitance and xylem hydraulic safety in four tall conifer species. *Plant, Cell &*

Environment, **37**, 1171–1183.

McElrone, A.J., Pockman, W.T., Martinez-Vilalta, J. & Jackson, R.B. (2004) Variation in xylem structure and function in stems and roots of trees to 20 m depth. *New Phytologist*, **163**, 507–517.

Meinzer, F.C., Lachenbruch, B. & Dawson, T.E. (2011) *Size- and age-related changes in tree structure and function* (eds Meinzer F.C., Lachenbruch B, and Dawson T.E.). Springer Netherlands, Dordrecht.

Mencuccini, M., Grace, J. & Fioravanti, M. (1997) Biomechanical and hydraulic determinants of tree structure in Scots pine: anatomical characteristics. *Tree Physiology*, **17**, 105–113.

Mitchell, M.D. & Denne, M.P. (1997) Variation in density of *Picea sitchensis* in relation to within-tree trends in tracheid diameter and wall thickness. *Forestry*, **70**, 47–60.

Myburg, A.A., Lev-Yadun, S. & Sederoff, R.R. (2013) Xylem Structure and Function. *eLS*, pp. 1–9. John Wiley & Sons, Ltd, Chichester, UK.

Nardini, A., Lo Gullo, M.A. & Salleo, S. (2011) Refilling embolized xylem conduits: Is it a matter of phloem unloading? *Plant Science*, **180**, 604–611.

Niklas, K.J. (2007) Maximum plant height and the biophysical factors that limit it. *Tree physiology*, **27**, 433–440.

Niklas, K.J. & Spatz, H. (2004) Growth and hydraulic (not mechanical) constraints govern the scaling of tree height and mass. , **101**, 15661–15663.

Olano, J.M., Arzac, A., García-Cervigón, A.I., von Arx, G. & Rozas, V. (2013) New star on the stage: amount of ray parenchyma in tree rings shows a link to climate. *The New phytologist*, **198**, 486–95.

Olson, M.E., Anfodillo, T., Rosell, J.A., Petit, G., Crivellaro, A., Isnard, S., León-Gómez, C., Alvarado-Cárdenas, L.O. & Castorena, M. (2014) Universal hydraulics of the flowering plants: vessel diameter scales with stem length across angiosperm lineages, habits and climates (ed B Enquist). *Ecology Letters*, **17**, 988–997.

Petit, G. & Anfodillo, T. (2009) Plant physiology in theory and practice: An analysis of the WBE

733 model for vascular plants. *Journal of Theoretical Biology*, **259**, 1–4.
734 Petit, G., Anfodillo, T., Carraro, V. & Grani, F. (2011) Hydraulic constraints limit height growth in
735 trees at high altitude. *New Phytologist*, **241-252**, 241–252.
736 Petit, G., Anfodillo, T. & De Zan, C. (2009) Degree of tapering of xylem conduits in stems and roots
737 of small *Pinus cembra* and *Larix decidua* trees. *Botany*, **87**, 501–508.
738 Petit, G., Pfautsch, S., Anfodillo, T. & Adams, M.A. (2010) The challenge of tree height in *Eucalyptus*
739 *regnans*: when xylem tapering overcomes hydraulic resistance. *New Phytologist*, **187**, 1146–
740 1153.
741 Petit, G., Anfodillo, T. & Mencuccini, M. (2008) Tapering of xylem conduits and hydraulic
742 limitations in sycamore (*Acer pseudoplatanus*) trees. *New Phytologist*, **177**, 653–664.
743 Pfautsch, S., Hölttä, T. & Mencuccini, M. (2015) Hydraulic functioning of tree stems—fusing ray
744 anatomy, radial transfer and capacitance. *Tree Physiology*, **35**, 706–722.
745 Pinheiro, J.C. & Bates, D.M. (2000) Linear Mixed-Effects Models: Basic concepts and examples.
746 *Mixed-Effects Models in S and S-PLUS*, pp. 3–56. Springer-Verlag, New York.
747 Pittermann, J., Sperry, J.S., Wheeler, J.K., Hacke, U.G. & Sikkema, E.H. (2006) Mechanical
748 reinforcement of tracheids compromises the hydraulic efficiency of conifer xylem. *Plant, Cell*
749 *and Environment*, **29**, 1618–1628.
750 Prendin, A.L., Petit, G., Carrer, M., Fonti, P., Björklund, J. & von Arx, G. (2017) New research
751 perspectives from a novel approach to quantify tracheid wall thickness. *Tree Physiology*.
752 Prendin, A.L., Petit, G., Fonti, P., Rixen, C., Dawes, M.A. & von Arx, G. (2017). Data from: Axial
753 xylem architecture of *Larix decidua* exposed to CO_2 enrichment and soil warming at the treeline.
754 Dryad Digital Repository. doi:10.5061/dryad.k6516.
755 R Development Core Team. (2014) R: A language and environment for statistical computing.
756 Rixen, C., Dawes, M.A., Wipf, S. & Hagedorn, F. (2012) Evidence of enhanced freezing damage in
757 treeline plants during six years of CO_2 enrichment and soil warming. *Oikos*, **121**, 1532–1543.
758 Rosner, S. (2013) Hydraulic and biomechanical optimization in norway spruce trunkwood - A review.

759 *IAWA Journal*, **34**, 365–390.
760 Rosner, S. & Karlsson, B. (2011) Hydraulic efficiency compromises compression strength
761 perpendicular to the grain in Norway spruce trunkwood. *Trees - Structure and Function*, **25**,
762 289–299.
763 Salleo, S., Trifilò, P., Esposito, S., Nardini, A. & Lo Gullo, M.A. (2009) Starch-to-sugar conversion
764 in wood parenchyma of field-growing *Laurus nobilis* plants: a component of the signal pathway
765 for embolism repair? *Functional Plant Biology*, **36**, 815.
766 Savage, V.M., Bentley, L.P., Enquist, B.J., Sperry, J.S., Smith, D.D., Reich, P.B. & von Allmen, E.I.
767 (2010) Hydraulic trade-offs and space filling enable better predictions of vascular structure and
768 function in plants. *Proceedings of the National Academy of Sciences*, **107**, 22722–22727.
769 Sperry, J.S., Meinzer, F.C. & McCulloh, K.A. (2008) Safety and efficiency conflicts in hydraulic
770 architecture: scaling from tissues to trees. *Plant, Cell & Environment*, **31**, 632–645.
771 Sperry, J.S., Nichols, K.L., Sullivan, J.E.M. & Eastlack, S.E. (1994) Xylem embolism in ring-porous,
772 diffuse-porous, and coniferous trees of Northern Utah and interior Alaska. *Ecology*, **75**, 1736–
773 1752.
774 Spicer, R. (2014) Symplasmic networks in secondary vascular tissues: parenchyma distribution and
775 activity supporting long-distance transport. *Journal of Experimental Botany*, **65**, 1829–1848.
776 Streit, K., Siegwolf, R.T.W., Hagedorn, F., Schaub, M. & Buchmann, N. (2014) Lack of
777 photosynthetic or stomatal regulation after 9 years of elevated [CO_2] and 4 years of soil warming
778 in two conifer species at the alpine treeline. *Plant, cell & environment*, **37**, 315–26.
779 Tyree, M.T. & Ewers, F.W. (1991) The hydraulic architecture of trees and other woody plants. *New*
780 *Phytologist*, **119**, 345–360.
781 Tyree, M.T. & Zimmermann, M.H. (2002) *Xylem structure and the ascent of sap*. Springer Berlin
782 Heidelberg, Berlin, Heidelberg.
783 West, G.B., Brown, J.H. & Enquist, B.J. (1999) A general model for the structure and allometry of
784 plant vascular systems. *Nature*, **400**, 664–667.

785 Wimmer, R. (2002) Wood anatomical features in tree rings as indicators of environmental change.
786 *Dendrochronologia*, **20**, 21–36.
787 Zar, J.H. (1999) Biostatistical analysis Fifth edition. *USA: Prentice Hall 4165*, **4159-4165**.
788 Ziemińska, K., Westoby, M. & Wright, I.J. (2015) Broad anatomical variation within a narrow wood
789 density range—A study of twig wood across 69 Australian angiosperms. *Plos One*, **10**,
790 e0124892.
791 Zuur, A.F., Ieno, E.N., Walker, N., Saveliev, A.A. & Smith, G.M. (2009) *Mixed effects models and*
792 *extensions in ecology with R*. Springer New York, New York, NY.
793
794
795

Figures

Fig. 1: Axial variability of functional traits as a function of distance from the apex (L) along the stem and root of the eight investigated *Larix decidua* trees. Left panels show the axial trends of (a) hydraulic diameter (Dh), (b) 5th percentile of cell wall reinforcement ($(t/b)^2$), (c) cell wall thickness of the latewood tracheids (CWT_{LW}) and (d) percentage of ray parenchyma ($PERPAR$). Each data point represents the trait value of a tree ring calculated for different positions along the tree axis (see Fig. S1b and Fig. S2a), with filled and open grey circles for the stem and root data, respectively. As an arbitrary example, red points/dots represent the axial variability (stem and root combined) in the tree ring of 2011 for a single tree (E3L1). Solid lines show the best fitting curves, whose details are reported in Table 3. In the right panels (e-g), the black lines denote the linear regression lines of the $\log_{10}$-$\log_{10}$ transformed variables for each selected functional trait ((e): Dh; (f): $(t/b)^2$, (g): CWT_{LW}) of control trees (A_{2001}, A). Coloured lines indicate the significant treatment effects (see Table 4 for details). (h) Mean ± 1 SE of $PERPAR$ grouped per treatment for stem (filled circles) and root (open squares), * $P< 0.05$. See Tables 1 and 2 for explanations of acronyms.

Fig. 2: Ontogenetic variation of the power scaling exponent b, corresponding to the axial trend in the general equation $y=aL^b$, for (a) Dh, (b) $(t/b)^2$ and (c) CWT_{LW} for the two control trees throughout the experiment (A1L1, A1L2; see Table 1). Only stem data for the period from 2001 to 2012, corresponding to tree age of 28 to 39 years and tree height of c. 1.1 to 2.6-3.6 m (see Fig. S1c), could be considered to avoid too few axial points for robust trend calculations. Solid curves indicate the best fitting regressions for the ontogenetic trend.

Fig. 3: Power scaling exponent b of the pairwise relationships between Dh, $(t/b)^2$ and CWT_{LW} as a function of cambial age of the tree rings in the stem (upper plots) and root (lower plots). Each symbol

821 represents $b \pm 95\%$ CI for all rings per 5-yr cambial age class and treatment as obtained from RMA
822 power fitting models. Power functions were used because they showed the best fit among the tested
823 functions. A negative value of b indicates a trade-off, a positive value a collinear change between any
824 two considered functional traits. Solid lines indicate the significant ($P<0.05$) linear regression through
825 all points irrespective of treatment as there were no treatment differences in the slope except for
826 PECSW (post-CO_2 soil warming) in the stem Dh vs. $(t/b)^2$ relationship.
827

828 Fig. 4: Variability of hydraulic carbon use efficiency (*HCUE*) with increasing distance from the apex
829 (L), based on $\log_{10}$-transformed data. The black line refers to the *HCUE* trend of control trees only,
830 whereas coloured lines indicate the significant treatment effects (see Table 3 for details).
831

832 Fig. 5: Relationship between the mean hydraulic diameter of apical tracheids (Dh_{APEX}: Dh at $L \leq 1$ cm)
833 and (a) ΔH (annual stem elongation rate) and (b) *RAI* (ring area index, i.e., the ring area (RA) at the
834 stem base standardized to remove the general axial pattern of RA vs. L, see Table 2). Solid lines
835 represent the fitted linear regressions.

Tables

Table 1: Timeline of the treatments and their combinations during the FACE and soil warming experiment at Stillberg (Davos, Switzerland). A_{2001}: ambient conditions before the beginning of the experiment; A: ambient conditions (control); EC: elevated CO_2; SW: soil warming, ECSW: elevated CO_2 and soil warming, PECSW: post elevated CO_2 and soil warming; PEC: post elevated CO_2 at ambient conditions.

	Trees	1983-2000	2001	2002	2003	2004	2005	2006	2007	2008	2009	2010	2011	2012
Combined treatments	E1L1 E2L2	A_{2001}	EC						ECSW			PECSW		
	E1L2 E3L1	A_{2001}	EC									PEC		
	A1L1 A2L2	A_{2001}	A						SW					
	A1L2 A2L1	A_{2001}	A											

842 Table 2: Acronyms and descriptions of variables used in this study.

Variable		Unit	Description	Function	Reference
Descriptive	***L***	cm	Distance from the apex	-	
	H	cm	Tree height	-	
Functional traits	***Dh*** ***Dh_{STEM}*** ***Dh_{ROOT}*** ***Dh_{APEX}***	µm	Tracheid hydraulic diameter - in the stem - in the root - in a ring corresponding to cambial age = 1	Hydraulic efficiency	Kolb & Sperry, 1999
	$(t/b)^2$	-	cell wall reinforcement (in this study: 5th percentile of values calculated in earlywood)	Hydraulic safety	Hacke *et al*., 2001
	CWT_{LW}	µm	Cell wall thickness of latewood tracheids (proxy for density)	Mechanical support	Myburg *et al.*, 2013
	CWA	μm^2	Cell wall area accumulated for the entire ring	Mechanical support	
	PERPAR ***$PERPAR_{STEM}$*** ***$PERPAR_{ROOT}$***	%	Percentage area of ray parenchyma cells on tangential section: - in the stem - in the root	Metabolic functions, e.g., capacity of carbon & water storage and radial transport	Spicer *et al*., 2014; von Arx *et al*., 2015
	Kh	$kg \cdot m \cdot MPa^{-1} \cdot s^{-1}$	Total conductivity	Hydraulic efficiency	Tyree & Zimmermann, 2002
Economics	***HCUE***	$kg \cdot m \cdot MPa^{-1} \cdot s^{-1} \cdot \mu m^{-2}$	Hydraulic carbon use efficiency: *Kh/CWA*	-	
Growth	***ΔH***	cm	Annual stem elongation	-	
	RA	μm^2	Ring area		
	RAI	-	Annual ring area index (*RA* standardized to remove the general axial pattern)	-	

843

Table 3: Linear, power and exponential fitting parameters (mean ± 1 standard error) *a*: *y*-intercept, *b*: slope), coefficient of determination (R^2) and significance (*P*) of the relationships assessed for the different trait variables. Relationships were only assessed for control trees not undergoing any CO_2 enrichment or soil warming treatment (A_{2001} and A; n=8 trees until 2001, n=4 from 2001 to 2006, n=2 from 2007 to 2012). See Table 2 for explanations of acronyms.

		Linear (y = a + b × x)				**Power ($Log_{10}(y) = Log_{10}(a) + b \times Log_{10}(x)$)**				**Exponential ($y = a + x^b$)**			
		a	***b***	***R²***	***P***	**$Log_{10}(a)$**	***b***	***R²***	***P***	***a***	***b***	***R²***	***P***
Axial variation	*Dh* vs. *L*	14.90 ± 0.21	$0.07 \pm 2.25\times10^{-3}$	0.72	<0.001	1.00 ± 0.01	0.17 ± 0.01	0.81	<0.001	2.86 ± 0.02	$2.18\times10^{-3} \pm 1.28\times10^{-4}$	0.66	<0.001
	$(t/b)^2$ vs. *L*	$0.02 \pm 4.17\times10^{-4}$	$-5.63\times10^{-5} \pm 4.5\times10^{-6}$	0.31	<0.001	-1.50 ± 0.02	-0.15 ± 0.01	0.46	<0.001	-3.81 ± 0.04	$-2.62\times10^{-3} \pm 3.35\times10^{-4}$	0.28	<0.001
	CWT_{LW} vs. *L*	3.35 ± 0.05	$4.09\times10^{-3} \pm 5.35\times10^{-4}$	0.15	<0.001	0.47 ± 0.01	0.05 ± 0.01	0.16	<0.001	1.22 ± 0.03	$1.02\times10^{-3} \pm 1.38\times10^{-4}$	0.15	<0.001
Economics	*HCUE* vs. *L*	$1.64\times10^{-15} \pm 2.24\times10^{-16}$	$2.52\times10^{-17} \pm 2.42\times10^{-18}$	0.25	<0.001	-15.22 ± 0.04	0.46 ± 0.02	0.44	<0.001	-2.99 ± 0.06	$-0.03 \pm 1.78\times10^{-3}$	0.21	<0.001
Growth	ΔH vs. Dh_{APEX}	-9.37 ± 7.88	1.78 ± 0.70	0.20	0.017	-1.20 ± 0.61	2.02 ± 0.58	0.31	<0.001	0.57 ± 0.91	0.16 ± 0.07	0.21	0.007
	RAI vs. Dh_{APEX}	0.71 ± 0.07	0.02 ± 0.01	0.34	<0.001	-0.30 ± 0.07	0.27 ± 0.07	0.36	<0.001	-0.29 ± 0.07	$0.02 \pm 6.20\times10^{-3}$	0.33	<0.001

Table 4: Results of the optimal linear mixed-effect models predicting the treatment effects on the different functional and carbon cost traits and the interaction between treatment and $Log_{10}L$ (see methods for details). Numbers indicate the estimates ± 1 SE. Significant terms are highlighted in bold. See Table 1 and 2 for explanations of acronyms. * $P< 0.05$, ** $P< 0.01$ and *** $P< 0.001$.

	Functional traits				**Carbon costs**
Fixed effects	**$Log_{10}Dh_{STEM}$**	**$Log_{10}Dh_{ROOT}$**	**$Log_{10}(t/b)^2$**	**$Log_{10}CWT_{LW}$**	**$Log_{10}HCUE$**
Intercept (A)	**0.82 ± 0.06*** **	**1.45 ± 0.05*** **	**-1.52 ± 0.04*** **	**0.49 ± 0.02*** **	**-18.34 ± 0.07*** **
$Log_{10}L$ (A)	**0.18 ± 0.01*** **	**0.04±0.02***	**-0.13 ± 0.01*** **	**0.04 ± 0.01 *** **	**0.3 ± 0.02*** **
$Log_{10}Dh_{APEX}$ (A)	**0.15 ±0.06****	-	-	-	-
A_{2001}	-	**0.03 ± 0.01****	0.03 ± 0.03	-0.04 ± 0.02	**-0.09 ± 0.05***
EC	-	0.00 ± 0.01	0.05 ± 0.04	-0.04 ± 0.03	0.08 ± 0.06
ECSW	-	**-0.06 ± 0.02*** **	**-0.28 ± 0.06*** **	**-0.15 ± 0.05****	**0.52 ± 0.11****
SW	-	**-0.04 ± 0.01*** **	-0.05 ± 0.04	0.02 ± 0.03	-0.11 ± 0.07
PECSW	-	**-0.03 ± 0.02***	**-0.38 ± 0.09*** **	**-0.25 ± 0.07*** **	**0.75 ± 0.17*** **
PEC	-	**-0.04 ± 0.02***	0.07 ± 0.12	-0.16 ± 0.09	**0.06 ± 0.2**
$Log_{10}L \times A_{2001}$	-	-	-0.01 ± 0.02	0.02 ± 0.01	**0.06 ± 0.03***
$Log_{10}L \times$ EC	-	-	-0.03 ± 0.02	0.02 ± 0.01	-0.02 ± 0.03
$Log_{10}L \times$ ECSW	-	-	**0.13 ± 0.03*** **	**0.08 ± 0.02*** **	**-0.23 ± 0.05*** **
$Log_{10}L \times$ SW	-	-	0.01 ± 0.02	0.01 ± 0.02	0.04 ± 0.03
$Log_{10}L \times$ PECSW	-	-	**0.15 ± 0.04*** **	**0.10 ± 0.03*** **	**-0.26 ± 0.08****
$Log_{10}L \times$ PEC	-	-	-0.06 ± 0.05	0.05 ± 0.04	0.08± 0.09

853 Figure 1

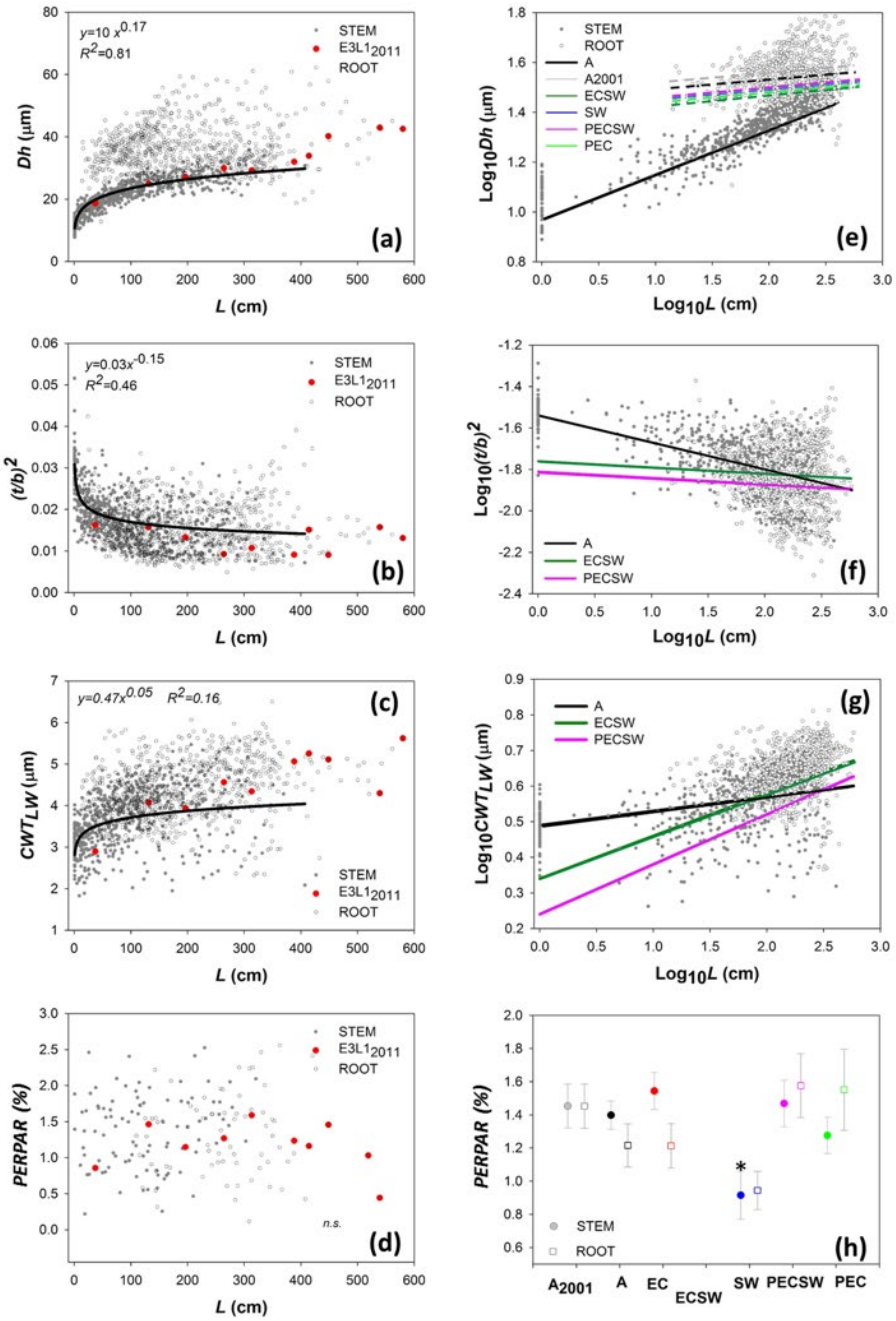

854

855

856 Figure 2

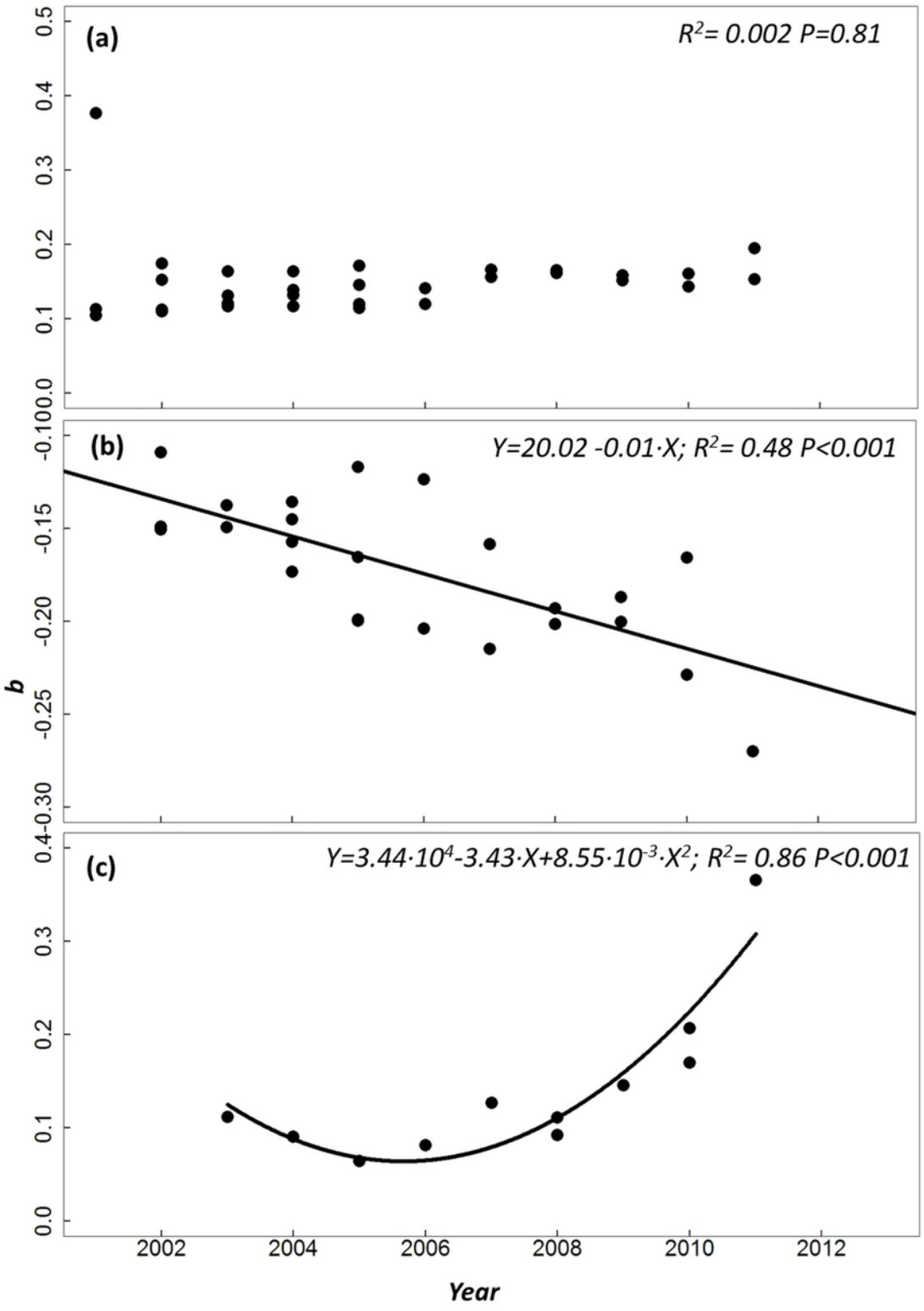

857

858

859 Figure 3

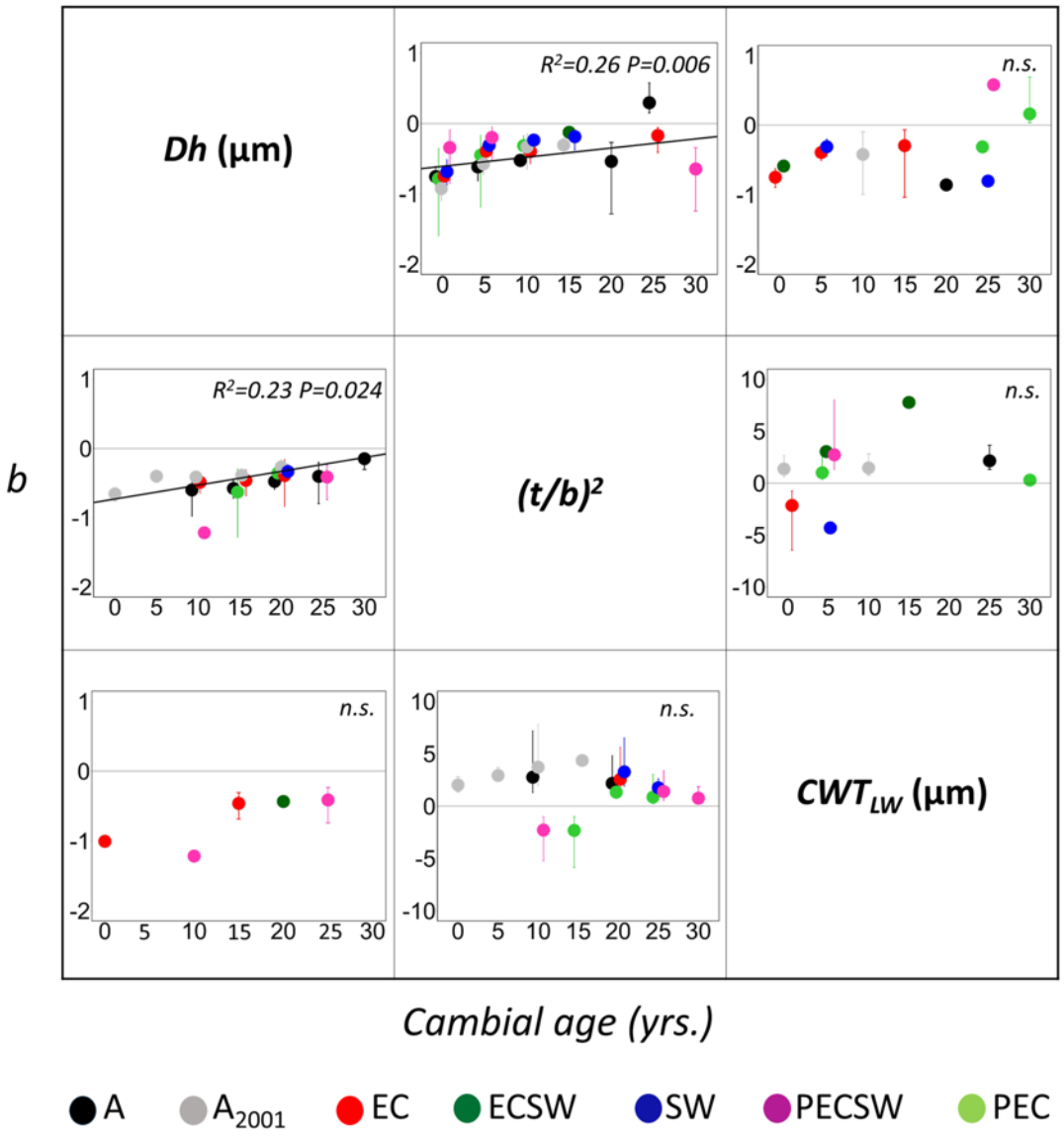

860

861

862 Figure 4

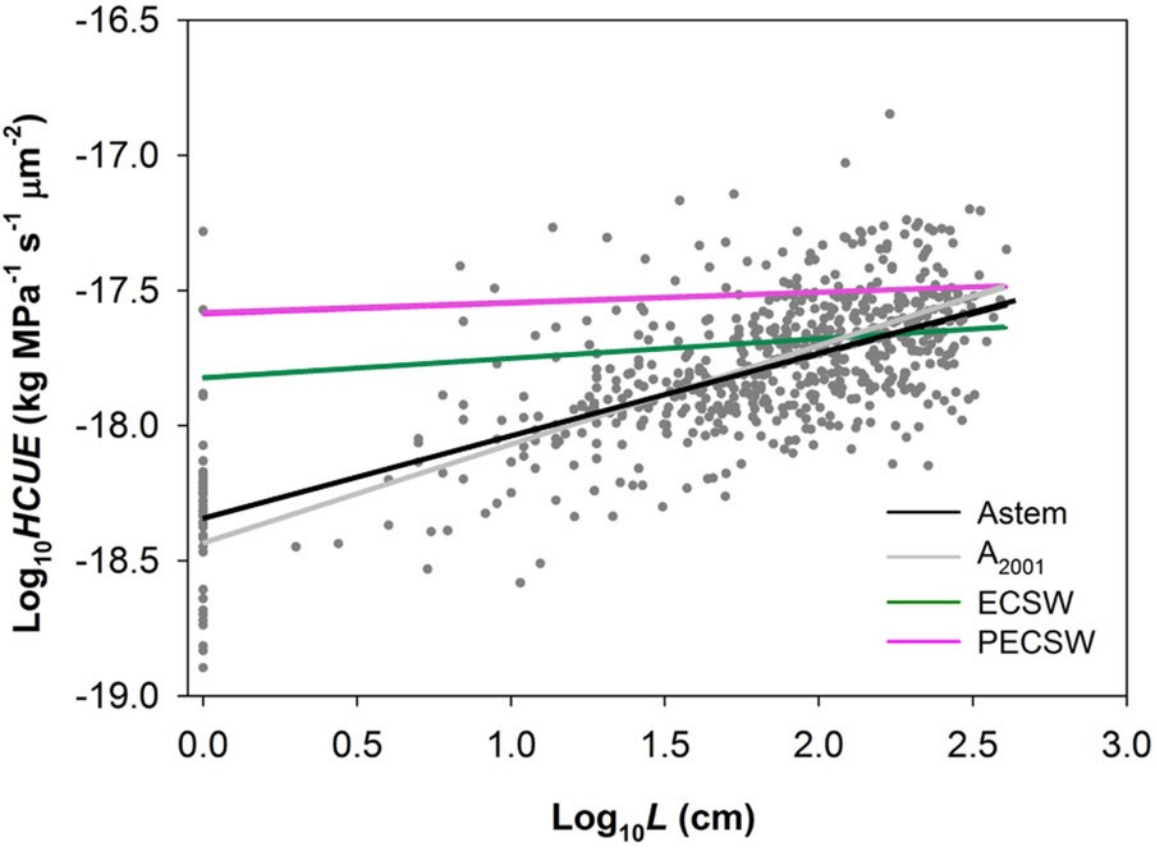

863

864 Figure 5

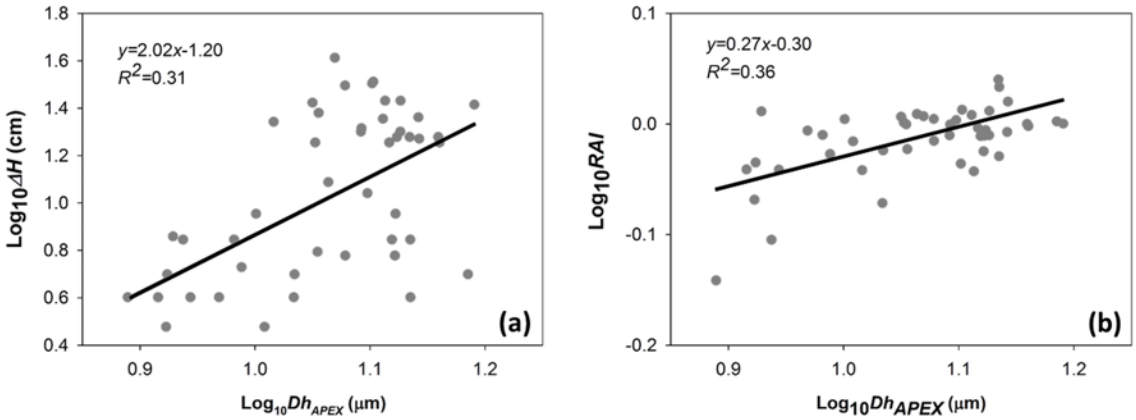

865